*Journal of Coordination Chemistry*
Vol. 65, No. 14, 20 July 2012, 2489–2499

Taylor & Francis
Taylor & Francis Group



# Isolation, crystal structure, and cytotoxicity on osteosarcoma of a ruthenium(III) complex with coordinated acetonitrile

JOANA MARQUES†, JOSÉ A. FERNANDES†, FILIPE A. ALMEIDA PAZ†, MARIA PAULA M. MARQUES‡ and SUSANA S. BRAGA*†

†Departamento de Química & CICECO, Universidade de Aveiro, 3810-193 Aveiro, Portugal
‡Departamento de Bioquímica, Faculdade de Ciências e Tecnologia, Universidade de Coimbra, PO Box 3126, 3001-401 Coimbra, Portugal

(*Received 1 March 2012; in final form 7 May 2012*)

The precursor Ru([9]aneS$_3$)(DMSO)Cl$_2$ (**1**), where [9]aneS$_3$ represents 1,4,7-trithiacyclononane, was dissolved in acetonitrile at 50°C and stirred for several hours to assess the solvent's ability to coordinate to **1**. A bis(acetonitrile) Ru(III) compound (**2**) crystallized as solid yellow needles upon slow evaporation of the reaction solution at room temperature. The structure of **2** was investigated in the solid state by FT-IR and single-crystal diffraction, showing it to be [Ru(III)([9]aneS$_3$)(NCMe)$_2$Cl]Cl$_2 \cdot 2$H$_2$O (**2**). To assess the biological action of **2**, growth-inhibition tests were carried by the MTT assay on a human tumor cell line of interest to our group, the osteosarcoma MG-63 line. Results have shown that the complex requires concentrations above 200 μmol L$^{-1}$ at 72 h of incubation to display cytotoxic action on this cell line.

*Keywords*: Ruthenium trithiacyclononane complexes; Acetonitrile; Single-crystal X-ray diffraction; Cytotoxicity evaluation

## 1. Introduction

Ruthenium trithiacyclononane (or [9]aneS$_3$) complexes, proposed as suitable alternatives for the cytotoxic Ru(II) arenes [1], are commonly prepared from the precursor Ru([9]aneS$_3$)(DMSO)Cl$_2$ (**1**). Relevant compounds of this family are the DNA intercalating agent [Ru([9]aneS$_3$)(dppz)Cl]$^+$ [2], the bactericidal [Ru([9]aneS$_3$)(phen)Cl]Cl [3], and the bioinorganic complex [Ru([9]aneS$_3$)(glycine)Cl], with mild antitumoral activity against the osteosarcoma MG-63 line after 72 h of incubation [4].

Acetonitrile is a solvent with mild coordinating properties, affording complexes with labile ligands. This work investigated the transformation of precursor **1** into an acetonitrile complex by slow crystallization of their mixed solution. An Ru(III) trithiacyclononane bis(acetonitrile) complex (**2**) was obtained. The Ru(III) oxidation state is unprecedented in ruthenium complexes of this family. Acetonitrile complexes

*Corresponding author. Email: sbraga@ua.pt

*Journal of Coordination Chemistry*
ISSN 0095-8972 print/ISSN 1029-0389 online 
http://dx.doi.org/10.1080/00958972.2012.696624

are also typically Ru(II), as the analog [Ru(II)([9]aneS$_3$)(NCMe)$_3$][$CF_3SO_3$]$_2$ [5] or the tris(acetonitrile) piano-stool organometallic complexes [Ru(II)($\eta^5$-cyclopentadienyl)(NCMe)$_3$][$PF_6$]$_2$ [6] and [Ru(II)($\eta^5$-2,4-dimethylpentadienyl)(NCMe)$_3$][$PF_6$]$_2$ [7].

Ruthenium(III) complexes have attracted strong research interest as potential anticancer agents [8]. This research was impelled by the success of NAMI-A (imidazolium *trans*-[tetrachloro(dimethylsulfoxide)(imidazole) ruthenate(III)]) [9] and KP1019 (indazolium *trans*-[tetrachlorobis(indazole)ruthenate(III)]) [10], which are currently in phase I/IIa clinical trials. NAMI-A was found to be particularly active against the development and growth of metastases of solid tumors [11], whereas KP1019 has shown direct antitumor activity against a wide range of primary explants of human tumors by inducing apoptosis [12]. The herein described Ru(III) bis(acetonitrile) complex (**2**) is thus expected to work as a suitable precursor for a new family of Ru(III) trithiacyclononane cytotoxic agents. Ruthenium cyanide and acetonitrile complexes are very useful starting materials; a tricyanoruthenium(III) linear building block was recently reported [13] and the use of acetonitrile as a leaving group permitted the preparation of a family of ruthenium pyridocarbazole compounds with inhibitory action on a collection of protein kinases [14].

## 2. Experimental

### 2.1. *General comments*

The precursor Ru([9]aneS$_3$)(DMSO)Cl$_2$ (**1**) was prepared from [Ru(DMSO)$_4$Cl$_2$] and 1,4,7-trithiacyclonane or [9]aneS$_3$ (from Fluka) as described in previous work [3]. Culture media (MEM) for the cytotoxicity experiments (details below), antibiotics (penicillin-streptomycin 100x solution), fetal bovine serum (FBS), MTT (3-(4,5-dimethylthiazol-2-yl)-2,5-diphenyl-2H-tetrazolium bromide), trypsin, and inorganic salts and acids (of analytical grade) were purchased from Sigma-Aldrich Chemical Co. The human osteosarcoma cancer cell line (MG-63) was kindly provided by the Associate Laboratory IBMC-INEB, Portugal.

Mass spectra were acquired with a Micromass Q-Tof II equipped with a Z-spray source, an electrospray probe and a syringe pump, and water was employed as eluent. Thermogravimetric analysis (TGA) studies were carried out using a Shimadzu TGA-50 system at a heating rate of 5°C min$^{-1}$ under air. Infrared spectra were recorded on a Unican Mattson Mod 7000 FT-IR spectrophotometer using KBr pellets; the spectrum of acetonitrile was collected by placing a drop of the solvent between two thin KBr pellets.

Optical photographs were taken on a Stemi 2000 stereomicroscope equipped with Carl Zeiss lenses and a digital high-resolution AxioCam MRc5 digital camera connected to a personal computer.

### 2.2. *Preparation of [Ru(III)([9]aneS$_3$)(NCMe)$_2$Cl]Cl$_2$·2H$_2$O (2)*

A saturated solution of Ru([9]aneS$_3$)(DMSO)Cl$_2$ (**1**) (roughly 100 mg, 0.23 mmol) in acetonitrile (50 mL) at 50°C was stirred for 20 h. The resulting pristine yellow solution was allowed to cool to ambient temperature and set to slowly evaporate over several

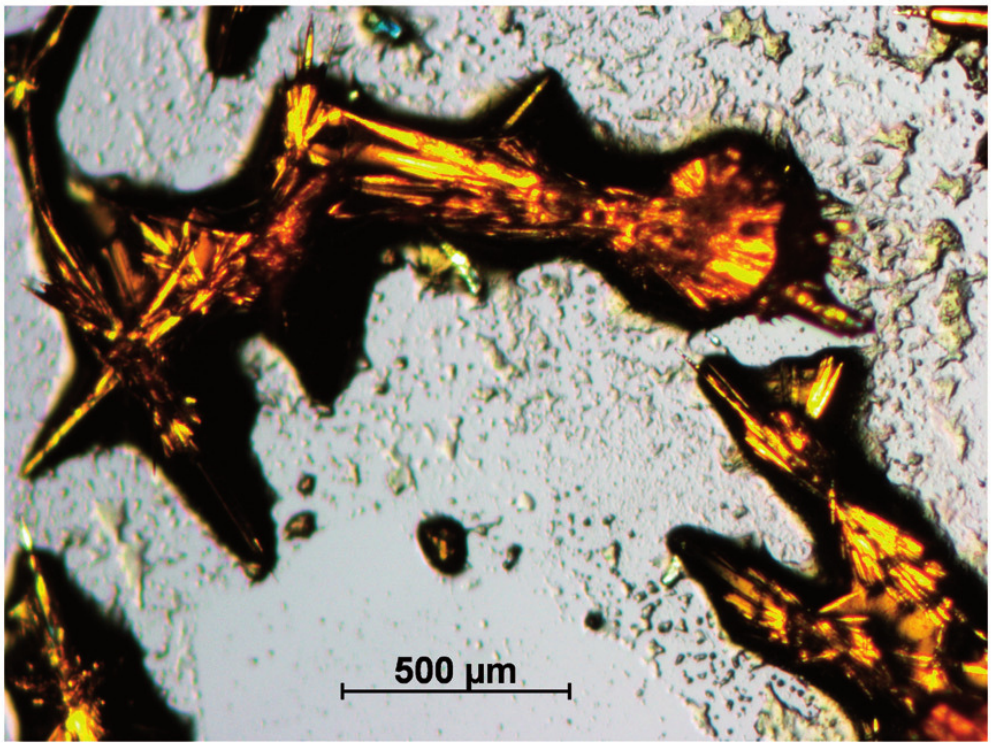


Figure 1. Needle-like morphology observed in the crystals of complex [Ru(III)([9]aneS$_3$)(NCMe)$_2$Cl]Cl$_2 \cdot 2H_2O$ (**2**).

days to obtain crystalline yellow needles (depicted in figure 1). ES-MS ($m/z$): 435.9 [$M^+$–Cl], 470.8 [$M^+$]. FT-IR (KBr pellets, $cm^{-1}$): $\bar{\nu} = 2984$ m, 2960 vs, 2921 vs, 2853 s, 2067 m, 1451 s, 1413 vs, 1302 m, 1290 m, 1262 m, 1240 m, 1170 m, 1083 s, 1035 s, 1023 s, 963 m, 940 m, 913 m, 823 s, 716 m, 678 m, 618 m, 568 m, 548 m, 521 m, 503 m, 483 m, 472 m, 456 m, 419 m, 398 m, 384 m, 375 m, 351 m, 336 m, 328 m, 324 m.

### 2.3. *Single-crystal X-ray diffraction studies*

Single-crystals of [Ru(III)([9]aneS$_3$)(NCMe)$_2$Cl]Cl$_2 \cdot 2H_2O$ (**2**) directly harvested from the crystallization vials were immediately immersed in highly viscous FOMBLIN Y perfluoropolyether vacuum oil (LVAC 140/13, Sigma-Aldrich) to avoid degradation caused by evaporation of the solvent. Crystals were mounted on a Hampton Research CryoLoop with the help of a Stemi 2000 stereomicroscope equipped with Carl Zeiss lenses [15]. Data were collected on a Bruker X8 Kappa APEX II CCD area-detector diffractometer (Mo-K$\alpha$ graphite-monochromated radiation, $\lambda = 0.71073$ Å) controlled by the APEX2 software package [16] and equipped with an Oxford Cryosystems Series 700 cryostream monitored remotely using the software interface Cryopad [17]. Images were processed using the software package SAINT+ [18] and data were corrected for absorption by the multiscan semiempirical method implemented in SADABS [19].

The structure was solved using the Patterson synthesis algorithm implemented in SHELXS-97 [20], allowing immediate location of the ruthenium metallic center and most of the heaviest atoms. All remaining non-hydrogen atoms were located from difference Fourier maps calculated from successive full-matrix least-squares refinement

Table 1. Crystal and structure refinement data for [Ru(III)([9]aneS$_3$)(NCMe)$_2$Cl]Cl$_2\cdot$2H$_2$O (**2**).

| | |
|---|---|
| Empirical Formula | $C_{10}H_{22}Cl_3N_2O_2RuS_3$ |
| Formula weight | 505.90 |
| Crystal system | Monoclinic |
| Space group | $P2_1/n$ |
| Unit cell dimensions (Å, °) | |
| $a$ | 7.4413(13) |
| $b$ | 11.690(2) |
| $c$ | 22.226(4) |
| $\beta$ | 98.088(9) |
| Volume (Å$^3$), $Z$ | 1914.2(6), 4 |
| Calculated density (g cm$^{-3}$) | 1.755 |
| Absorption coefficient (mm$^{-1}$) | 1.568 |
| Crystal size (mm$^3$) | $0.12 \times 0.08 \times 0.03$ |
| Crystal type | Yellow block |
| $\theta$ range for data collection (°) | 3.56–29.13 |
| Limiting indices | $-9 \le h \le 10$;<br>$-16 \le k \le 16$;<br>$-30 \le l \le 30$ |
| Reflections collected | 1,08,341 |
| Independent reflections | 5123 [$R$(int) = 0.0659] |
| Completeness to $\theta = 29.13$ (%) | 99.8 |
| Final $R$ indices [$I > 2\sigma(I)$][a,b] | $R_1 = 0.0489$,<br>$wR_2 = 0.1226$ |
| Final $R$ indices (all data)[a,b] | $R_1 = 0.0593$,<br>$wR_2 = 0.1291$ |
| Weighting scheme[c] | $m = 0.0563$<br>$n = 9.1512$ |
| Largest difference peak and hole (eÅ$^{-3}$) | 1.050 and −1.475 |

[a] $R_1 = \sum||F_o| - |F_c||/\sum|F_o|$; [b] $wR_2 = \sqrt{\sum[w(F_o^2 - F_c^2)^2]/\sum[w(F_o^2)^2]}$;
[c] $w = 1/[\sigma^2(F_o^{2])+(mP)^2+nP]}$, where $P = (F_o^2 + 2F_c^2)/3$.

cycles on $F^2$ using SHELXL-97 [20a, 21]. All non-hydrogen atoms were successfully refined using anisotropic displacement parameters.

Hydrogen atoms bound to carbon were placed at their idealized positions using appropriate *HFIX* instructions in SHELXL: 137 for the terminal $CH_3$ methyl groups belonging to the acetonitrile ligands and 23 for $CH_2$ groups belonging to the [9]aneS$_3$ ligand. All these atoms were included in subsequent refinement cycles in riding motion approximation with isotropic thermal displacements parameters ($U_{iso}$) fixed at $1.5 \times U_{eq}$ of the parent carbon.

The last difference Fourier map synthesis showed the highest peak (1.050 eÅ$^{-3}$) and deepest hole (−1.475 eÅ$^{-3}$) located at 0.41 and 0.55 Å from C1 and Cl2, respectively.

Information concerning crystallographic data collection and structure refinement details is summarized in table 1.

## 2.4. *Toxicity and cell viability evaluation*

**2.4.1. Preparation of solutions for biological assays.** Solutions of **2** were prepared at concentrations ranging from $5.0 \times 10^{-5}$ to $4.0 \times 10^{-4}$ mol L$^{-1}$ in cell culture medium (MEM, see description below). MTT (3-[4,5-dimethylthiazol-2-yl]-2,5-diphenyltetrazolium bromide) was prepared in a concentration of 5 mg mL$^{-1}$ in sterile phosphate buffered saline.

**2.4.2. Cell culture.** Stock cultures of MG-63 were maintained at 37°C in a humidified atmosphere under 5% $CO_2$. MG-63 cells (grown in monolayers) were kept in Eagle's Minimum Essential Medium (MEM, an aqueous nutrient solution) supplemented with 10% heat-inactivated FBS, 1 mmol $L^{-1}$ sodium pyruvate, non-essential amino acids and antibiotics (100 units of penicillin and 100 mg of streptomycin). The cell line was subcultured twice a week and harvested upon addition of trypsin/EDTA (0.05% trypsin/EDTA solution).

**2.4.3. Toxicity and cell viability assays.** Cell viability following exposure to **2** at 50, 100, 200, and 400 μmol $L^{-1}$ and 72 h of incubation was assessed by mitochondrial dehydrogenase activity – MTT colorimetric assay [22]. Three independent experiments with triplicates for each drug concentration were performed.

MG-63 cells were plated at a density of $1.1 \times 10^5$ cells $mL^{-1}$ on 48-well plates. Twenty-four hours after seeding, test solutions of **2** were added to the medium and the cultures were incubated at 37°C. After 72 h, 50 μL of MTT were added to each well and the plates were incubated at 37°C for 4 h, after which MTT was removed by aspiration, and the formazan crystals formed in the cells dissolved by addition of 400 μL of DMSO under agitation. Measurements were carried out with a microplate reader at a working wavelength of 550 nm.

**2.4.4. Statistical analysis.** All experiments were performed in triplicate. Results are expressed as a percentage of the control (100%) and represent the mean values ± standard deviation (the corresponding error bars are displayed in the graphical plots). Statistical analysis was performed by analysis of variance. Tukey's *post hoc* test was used for statistical comparison between the experimental data, *p*-values less than 0.05 having been considered as significant.

## 3. Results and discussion

Ruthenium acetonitrile complexes have sparked interest not only in attempts to understand the role of acetonitrile as a coordinating solvent, but also due to their superior performance as synthetic intermediates. $[Ru([9]aneS_3)(NCMe)_3][CF_3SO_3]_2$, which can be obtained from **1** by use of a chloride sequestering agent, $Ag(CF_3SO_3)$, in refluxing acetonitrile [6] was reported to react with pyridine (while **1** does not) to afford a mixture of $[Ru([9]aneS_3)(py)_2(NCMe)]^{2+}$ and $[Ru([9]aneS_3)(py)_3]^{2+}$ [23].

We herein show that the coordinating properties of acetonitrile allow it to bind to **1** under mild heating and in the absence of a chloride sequestering agent. The solid compound unexpectedly comprises an Ru(III) specimen, $[Ru([9]aneS_3)(NCMe)_2Cl]Cl_2$ (**2**). Although uncommon, oxidation of Ru(II) to Ru(III) in nitrile complexes is not unprecedented, being well-described in the complex cation $[Ru(NH_3)_5(NCMe)]^{2+}$ [24] and in $[Ru(NH_3)_5(NCR)]^{2+}$ (where NCR = isonicotinonitrile) [25].

### 3.1. *Vibrational spectroscopy (FT-IR)*

FT-IR spectra performed on the solid gave quick insight into the newly formed complex (**2**); the spectrum of the crystals exhibited new bands associated with

Table 2. Selected FT-IR data for **1** and **2**.

| Observed frequency ($cm^{-1}$) | | |
|---|---|---|
| **1** | **2** | Approximate description |
| – | 2853 | $\nu_{C-H}$ (NCMe)[a] |
| – | 2067 | $\nu_{C\equiv N}$[b] |
| 1448 | 1452 | $\delta_{CH}$ ([9]aneS$_3$) |
| 1402,1415(sh) | 1415 | $\delta_{CH}$ ([9]aneS$_3$) |
| – | 1035 | $\rho_{CH}$ (NCMe) [26] |
| – | 521, 503 | $\nu_{Ru-N}$[c] |

[a]Observed at 2867 $cm^{-1}$ for pure NCMe, assigned as in ref. [26].
[b]Observed at 2251 and 2254 $cm^{-1}$ for pure acetonitrile.
[c]By comparison to the Ru–$N_2$ band (504 $cm^{-1}$ in $[RuN_2(NH_3)_5]Cl_2$) [27].

incorporation of NCMe and some changes in the vibrations of the [9]aneS$_3$ macrocycle. The main features are summarized in table 2.

The C≡N stretching bands in **2** are strongly redshifted in regard to those observed in the pure solvent, which indicates coordination. In particular, a shift in the red direction has been associated with interaction of NCMe with Lewis acids such as metal cations [28]. The bands at 525–500 $cm^{-1}$ are associated with the Ru–N bond, thus presenting further evidence of NCMe coordination.

Ru(II) complexes with NCMe often present blueshifts for the C≡N stretch, associated with back-donating effects of Ru(II); for instance, in Ru($\eta^5$-2,4-dimethylpentadienyl)(NCMe)$_3$]$BF_4$ (from [5]) these bands are observed at 2313 and 2277 $cm^{-1}$, whereas back donation is absent in Ru(III) complexes and the higher oxidation state of Ru(III) affords stronger Lewis acid character. This theory accounts for the features of the CN stretch observed in **2** and further evidences for Ru(III) oxidation state.

### 3.2. *Thermogravimetry*

TGA of **2** was compared to that of **1** (data collected in previous work [3]), as depicted in figure 2. The results are clearly indicative of replacement of DMSO ligands (boiling at 189°C in the pure state) by the NCMe (pure acetonitrile has a boiling point around 82°C). Weight loss of **2** of *ca* 5.2% occurs from room temperature to 125°C, whereas the precursor had no mass loss in this temperature range. This step for **2** can be associated with the removal of hydration water and/or partial loss of acetonitrile. A similar thermal phenomenon was observed on a rhenium acetonitrile complex, [Re(bipy)(CO)$_3$(NCMe)][$CF_3SO_3$], and ascribed to loss of labile NCMe [29].

No further mass loss was observed until 250°C, at which **1** and **2** decompose with an abrupt mass loss until 290°C. The residues of **1** suffered a second, smoother decomposition from 330°C to 460°C, while the residues of **2** were more reactive, undergoing oxidation with mass increase from 325°C to 430°C, and slowly decomposing afterward to leave a residual mass of 35% at 480°C.

### 3.3. *Crystal structure description of [Ru(III)([9]aneS$_3$)(NCMe)$_2$Cl]Cl$_2$ · 2H$_2$O (2)*

Compound **2**, formulated as [Ru(III)([9]aneS$_3$)(NCMe)$_2$Cl]$Cl_2 \cdot 2H_2O$ on the basis of single-crystal X-ray diffraction studies (table 1), crystallizes in the monoclinic space

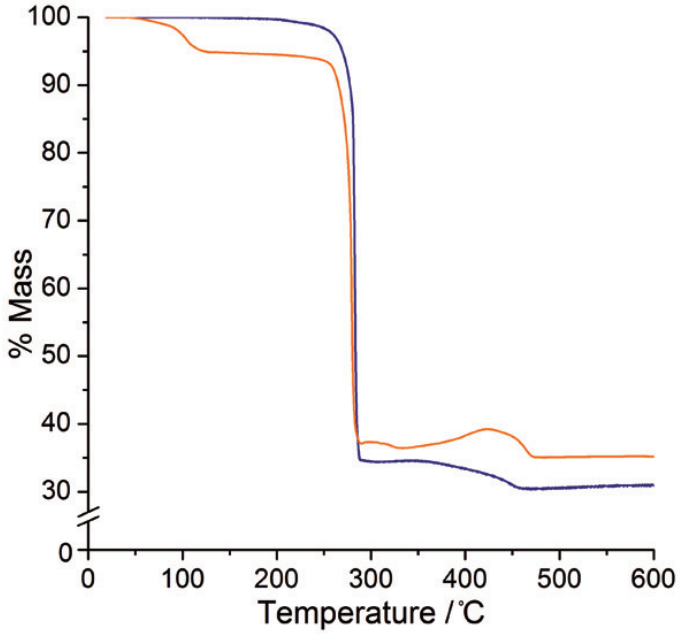


Figure 2. TG traces for the ruthenium precursor complex **1** (darker solid line) and the bis(acetonitrile) complex **2** (lighter solid line, orange on the online version).

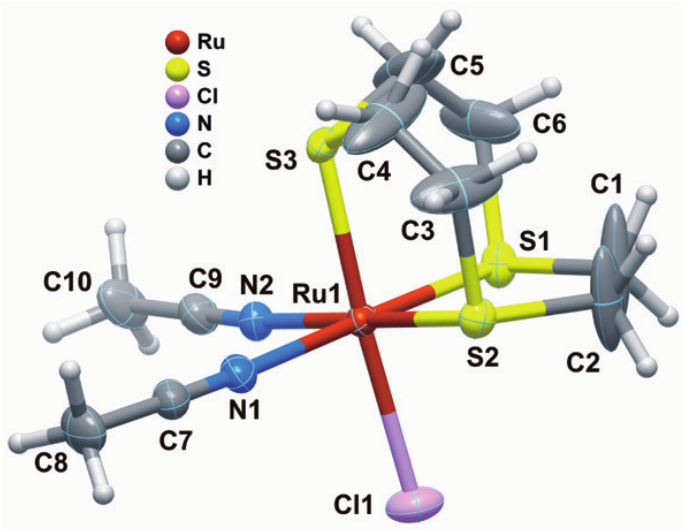


Figure 3. Schematic representation of the $[Ru([9]aneS_3)(NCMe)_2Cl]^{2+}$ cation composing the crystal structure of **2**. Thermal ellipsoids are drawn at the 50% probability level and hydrogen atoms as small spheres with arbitrary radii.

group $P2_1/n$ with the asymmetric unit being composed of an $Ru^{3+}$ cation (figure 3). The coordination environment around the metal center can be envisaged as a distorted octahedron in which $[9]aneS_3$ occupies three *fac* coordination positions. The Ru–S distances range from 2.2829(11) to 2.2938(11) Å, the Ru–N are 2.078(4) and 2.083(4) Å, and the Ru–Cl is 2.4505(11) Å. The *cis* and *trans* internal octahedral angles were found in the 87.83(4)–92.20(10)° and 176.43(4)–179.74(11)° ranges, respectively, being close to the expected values for an ideal octahedral coordination environment.

Given the existence of several donors and acceptors, the crystal structure is rich in hydrogen-bonding interactions. As depicted in figure 4, both crystallization water

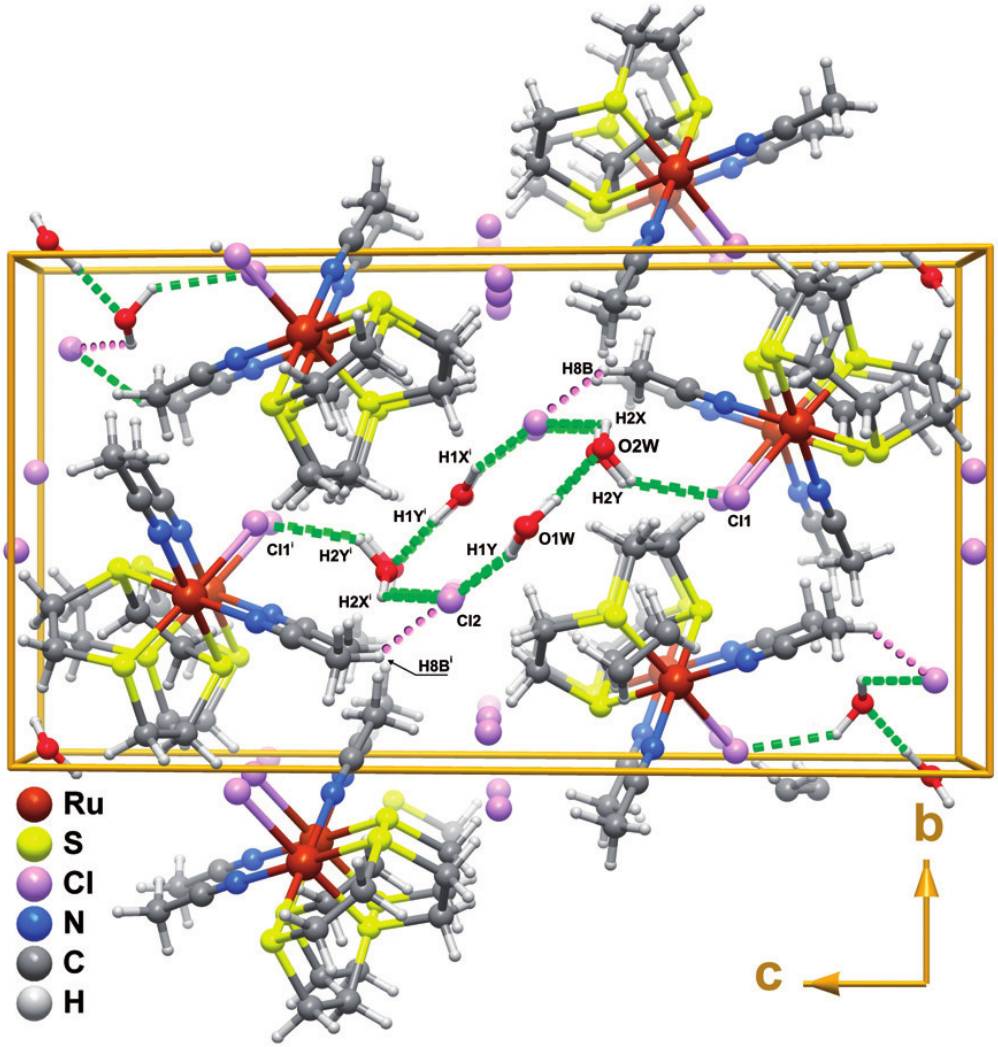


Figure 4. Crystal packing of [Ru(III)([9]aneS$_3$)(NCMe)$_2$Cl]Cl$_2$·2H$_2$O (**2**) viewed in perspective along the [100] crystallographic direction. Dashed lines emphasize the hydrogen-bonding interactions connecting water molecules and the cationic complexes. One chloride interacts with water *via* hydrogen bonds to form a motif described by the graph set $R_6^4$ (12) [30]. Geometrical details on these hydrogen-bonding interactions: O1W–H1X···O2W with $d_{O\ldots O}=2.710(7)$ Å and $<(OHO)=177(8)^\circ$; O2W–H2X···Cl2$^{i}$ with $d_{O\ldots Cl}=2.861(8)$ Å and $<(OHCl)=124(8)^\circ$; O1W–H1Y···Cl2 with $d_{Cl\ldots O}=2.897(6)$ Å and $<(OHCl)=158(6)^\circ$; O2W–H2Y···Cl1 with $d_{O\ldots Cl}=3.188(5)$ Å and $<(OHCl)=140(7)^\circ$. Another weak hydrogen-bonding interaction (dotted lines) is C8–H8B···Cl2$^{i}$ with $d_{C\ldots Cl}=3.650(6)$ Å and $<(CHCl)=143^\circ$. Symmetry transformations used to generate equivalent atoms: ($^{i}$) $2-x$, $1-y$, $1-z$.

molecules and one of the free chlorides (Cl2) interact *via* hydrogen bonds forming a centrosymmetric ring described by the graph set motif $R_6^4$ (12) [30], plus a hydrogen bond adjacent to the ring (dashed lines in figure 4). The distances D···A and angles D–H···A range from 2.710(7) to 3.188(5) Å and 124(8) to 177(8)°, respectively (D is the hydrogen donor and A is acceptor). Additionally, one weak hydrogen bond is adjacent to the ring, with a C···Cl distance of 3.650(6) Å and a C–H···Cl angle of *ca* 143° (dotted lines in figure 4).

### 3.4. *Cytotoxicity studies on osteosarcoma MG-63 cells*

The introduction of acetonitrile is not expected to bring, *per se*, toxicity to the ruthenium complex; still, nitrile-bearing cytotoxic copper complexes have been recently

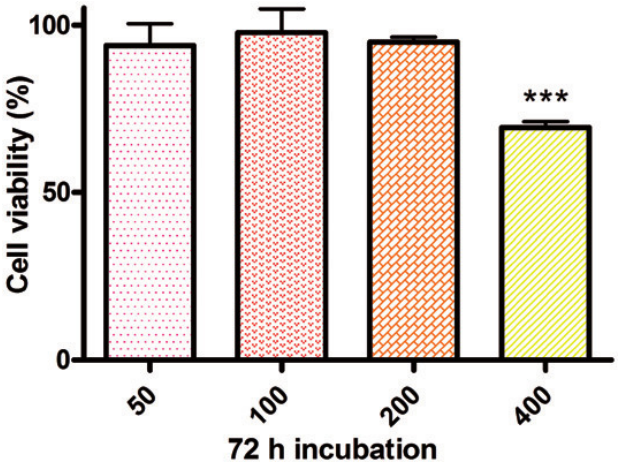


Figure 5. Cytotoxic effect of **2** at different concentrations and after 72 h of incubation on the human osteosarcoma line MG-63. The data are expressed as a percentage of the control (100%) and represent the average ± mean standard deviation from experiments carried out in triplicate; *** denotes $p$-value $< 0.001$.

reported [31]. It was thus found useful to establish the inertness of **2** in regard to cultured human cells.

The toxicity of **2** was studied by the *in vitro* MTT assay [22] on a human bone cancer line of interest to our group, the osteosarcoma MG-63 line. The cells were incubated for a period of 72 h with solutions of **2** in MEM at different concentrations, ranging from 50 to 200 μmol $L^{-1}$ and the viability was measured by colorimetric test (MTT). The results showed no significant cytotoxicity for these concentrations, so **2** could be classified as non-active; in fact, most drugs have an $IC_{50}$ below 100 μmol $L^{-1}$ (i.e., a 50% reduction in cell viability is observed at concentrations below 100 μmol $L^{-1}$).

We have, nonetheless, further tested **2** at a higher concentration – 400 μmol $L^{-1}$. At this very high dosage, there is indeed a coherent and significant growth inhibition, but it is worth noting that the cell count reduction did not lower by 50%. The global set of results, presented in figure 5, is thus characteristic of a marginal overall toxic activity, with an estimated $IC_{50} > 400$ μmol $L^{-1}$, lying well above the 100 μmol $L^{-1}$ considered useful for therapeutics.

## 4. Conclusions

Cytotoxic ruthenium complexes have long been explored for biological activity, either against microbe pathogens, as antimicrobials and antifungals [32, 33], or against human cancer. In particular, Ru(III) compounds have been on the spotlight for antitumoral action since the discovery of KP1019 and NAMI-A. To date, many Ru(III) cytotoxic compounds continue to emerge, bringing interesting new properties as superior apoptotic activity [34], or radical scavenging action [35]. Complex **2** reported here is the first within the Ru([9]ane$S_3$) family to present ruthenium in the +3 oxidation state, opening a new path for the preparation of such Ru(III) compounds.

*In vitro* tests showed that **2** has very low toxicity on MG-63 cells, constituting a precursor inert toward cells. Further optimization of the synthetic procedure using

solvothermal or microwave-assisted syntheses is in progress (aiming at reduced reaction and crystallization times).

Recent literature presents interesting examples on the preparation of cytotoxic Ru(III) complexes starting also from inert precursors $[RuX(EPh_3)_3]$ (with X = Cl, Br and E = As, P) and using Schiff-base ligands. The resulting complexes were able to match [36] or even surpass [37] the activity of the reference drugs against the tested pathogenic bacteria strains and allergenic fungal species. Future work will thus be dedicated to incorporation of active bidentate ligands into the backbone of **2**, by simple replacement of the acetonitriles. A rational approach will comprise organic ligands from natural sources wanting redox activation [38], aiming at ruthenium drugs of superior performance.



## Supplementary material

Crystallographic data (excluding structure factors) for the structure reported in this article have been deposited with the Cambridge Crystallographic Data Centre as supplementary publication No. CCDC-832949. Copies of the data can be obtained free of charge on application to CCDC, 12 Union Road, Cambridge CB2 2EZ, U.K; Fax: (+44) 1223 336033; E-mail: deposit@ccdc.cam.ac.uk

## Acknowledgments

We are grateful to the Fundação para a Ciência e a Tecnologia (FCT), Orçamento de Estado (OE), and Fundo Europeu de Desenvolvimento Regional (FEDER) through the program COMPETE (Programa Operacional Factores de Competitividade) for their general financial support and for specific funding toward the purchase of the single-crystal diffractometer. The FCT and the European Social Fund, through the Programma Operacional Potencial Humano (POPH), are acknowledged for a PhD grant to J.M. (SFRH/BD/44791/2008), and for a postdoc grant to J.A.F. (SFRH/BPD/63736/2009).

## References

[1] B. Serli, E. Zangrando, T. Gianferrara, C. Scolaro, P.J. Dyson, A. Bergamo, E. Alessio. *Eur. J. Inorg. Chem.*, 3423 (2005).
[2] T.M. Santos, J. Madureira, B.J. Goodfellow, M.G.B. Drew, J.P. Jesus, V. Felix. *Metal-Based Drugs*, **8**, 125 (2001).
[3] J. Marques, T.M. Braga, F.A.A. Paz, T.M. Santos, M.F.S. Lopes, S.S. Braga. *Biometals*, **22**, 541 (2009).
[4] J. Marques, T.M. Santos, M.P. Marques, S.S. Braga. *Dalton Trans.*, 9812 (2009).
[5] C. Landgrafe, W.S. Sheldrick. *J. Chem. Soc., Dalton Trans.*, 1885 (1994).
[6] W. Luginbuhl, P. Zbinden, P.A. Pittet, T. Armbruster, H.B. Burgi, A.E. Merbach, A. Ludt. *Inorg. Chem.*, **30**, 2350 (1991).
[7] T. Lumini, D.N. Cox, R. Roulet, K. Schenkand. *J. Organomet. Chem.*, **434**, 363 (1992).
[8] (a) M.J. Clarke. *Coord. Chem. Rev.*, **236**, 69 (2003); (b) M.J. Clarke, F. Zhu, D. Frasca. *Chem. Rev.*, **99**, 2511 (1999).

[9] G. Sava, R. Gagliardi, M. Cocchietto, K. Clerici, I. Capozzi, M. Marrella, E. Alessio, G. Mestroni, R. Milanino. *Pathol. Oncol. Res.*, **4**, 30 (1998).
[10] (a) F. Kraftz, N. Mulinacci, L. Messori, I. Bertini, B.K. Keppler. *Met. Ions Biol. Med.*, **2**, 69 (1992); (b) B.K. Keppler, K.G. Lipponer, B. Stenzel, F. Kratz. In *Metal Complexes in Cancer Chemotherapy*, B.K. Keppler (Ed.), VCH, Weinheim (1993), p. 187.
[11] (a) I. Bratsos, S. Jedner, T. Gianferrara, E. Alessio. *Chimia*, **61**, 692 (2007); (b) E. Alessio, G. Mestroni, A. Bergamo, G. Sava. *Met. Ions Biol. Sys.*, **42**, 323 (2004); (c) E. Alessio, G. Mestroni, A. Bergamo, G. Sava. *Curr. Topics Med. Chem.*, **4**, 1525 (2004); (d) M. Bacac, A.C.G. Hotze, K. von der Schilden, J.G. Haasnoot, S. Pacor, E. Alessio, G. Sava, J. Reedijk. *J. Inorg. Biochem.*, **98**, 402 (2004).
[12] (a) M.A. Jakupec, V.B. Arion, S. Kapitza, E. Reisner, A. Eichinger, M. Pongratz, B. Marian, N. Graf von Keyserlingk, B.K. Keppler. *Int. J. Clin. Pharmacol. Ther.*, **43**, 595 (2005); (b) C.G. Hartinger, M.A. Jakupec, S. Zorbas-Seifried, M. Groessl, W. Berger, H. Zorbas, P.J. Dyson, B.K. Keppler. *Chem. Biodiv.*, **5**, 2140 (2008).
[13] J. Xiang, W.L. Man, J. Guo, S.M. Yiu, G.H. Lee, S.M. Peng, G. Xu, S. Gao, T.C. Lau. *Chem. Commun.*, 6102 (2010).
[14] H. Bregman, P.J. Carroll, E. Meggers. *J. Am. Chem. Soc.*, **128**, 877 (2006).
[15] T. Kottke, D. Stalke. *J. Appl. Crystallogr.*, **26**, 615 (1993).
[16] APEX2. *Data Collection Software (Version 2.1-RC13)*, Bruker AXS, Delft, The Netherlands (2006).
[17] Cryopad. *Remote Monitoring and Control (Version 1.451)*, Oxford Cryosystems, Oxford, UK (2006).
[18] SAINT+. *Data Integration Engine (Version 7.23a)*, Bruker AXS, Madison, WI (2005).
[19] G.M. Sheldrick. *SADABS, Bruker/Siemens Area Detector Absorption Correction Program (Version 2.01)*, Bruker AXS, Madison, WI (1998).
[20] (a) G.M. Sheldrick. *Acta Crystallogr., Sect. A*, **64**, 112 (2008); (b) G.M. Sheldrick. *SHELXS-97, Program for Crystal Structure Solution*, University of Göttingen: Göttingen, Germany (1997).
[21] G.M. Sheldrick. *SHELXS-97, Program for Crystal Structure Refinement*, University of Göttingen, Göttingen, Germany (1997).
[22] T. Mosmann. *J. Immunol. Methods*, **65**, 55 (1983).
[23] E. Iengo, E. Zangrando, E. Baiutti, F. Munini, E. Alessio. *Eur. J. Inorg. Chem.*, 1019 (2005).
[24] S.E. Diamond, B. Grant, G.M. Tom, H. Taube. *Tetrahedron Lett.*, **15**, 4025 (1974).
[25] A.E.H. Machado, Z.N. Rocha, E. Tfouni. *J. Photochem. Photobiol. A: Chem.*, **88**, 85 (1995).
[26] J.M. Alía, H.G.M. Edwards. *J. Phys. Chem. A*, **109**, 7977 (2005).
[27] S.M. Vinogradova, M.G. Kaplunov, G. Yu, O. Borod'ko. *J. Struct. Chem.*, **13**, 56 (1972).
[28] W.R. Fawcett, G. Liu, T.E. Kessler. *J. Phys. Chem.*, **97**, 9293 (1993).
[29] F.E. Kühn, J.L. Zuo, F.F. Biani, A.M. Santos, Y. Zhang, J. Zhao, A. Sandulache, E. Herdtweck. *New J. Chem.*, **28**, 43 (2004).
[30] J. Grell, J. Berstein, G. Tinhofer. *Acta Crystallogr. B*, **55**, 1030 (1999).
[31] A. Zanella, V. Gandin, M. Porchia, F. Refosco, F. Tisato, F. Sorrentino, G. Scutari, M.P. Rigobello, C. Marzano. *Invest. New Drugs*, **29**, 1213 (2011).
[32] A.I. Ramos, T.M. Braga, S.S. Braga. *Mini-Rev. Med. Chem.*, **12**, 227 (2012).
[33] C.S. Devi, S. Satyanarayana. *J. Coord. Chem.*, **65**, 474 (2012).
[34] Z. Trávníček, M. Matiková-Malarová, R. Novotná, J. Vančo, K. Štěpánková, P. Suchý. *J. Inorg. Biochem.*, **105**, 937 (2011).
[35] R. Prabhakaran, P. Kalaivani, R. Jayakumar, M. Zeller, A.D. Hunter, S.V. Renukadevi, E. Ramachandran, K. Natajaran. *Metallomics*, **3**, 42 (2011).
[36] N.P. Priya, S. Arunachalam, N. Sathya, C. Jayabalakrishnan. *J. Coord. Chem.*, **63**, 1440 (2010).
[37] S. Arunachalam, N.P. Priya, C. Saravanakumar, C. Jayabalakrishnan, V. Chinnusamy. *J. Coord. Chem.*, **63**, 1795 (2010).
[38] One known example of this strategy is ferrocifen, a cytostatic agent inspired on the natural drug tamoxifen. It combines the redox abilities of the ferrocenyl moiety to the activity of the ligand and presents a wider range of action, including not only estrogen-dependent but also estrogen-independent tumors.